Influence of halide composition on the structural, electronic, and optical properties of mixed $CH_3NH_3Pb(I_{1-x}Br_x)_3$ perovskites calculated using the virtual crystal approximation method

Un-Gi Jong,[1] Chol-Jun Yu,[1,*] Jin-Song Ri,[1] Nam-Hyok Kim,[2] and Guk-Chol Ri[2]

[1]*Department of Computational Materials Design, Faculty of Materials Science, Kim Il Sung University, Ryongnam-Dong, Taesong District, Pyongyang, Democratic People's Republic of Korea*

[2]*Department of Theoretical Physics, Faculty of Physics, Kim Il Sung University, Ryongnam-Dong, Taesong District, Pyongyang, Democratic People's Republic of Korea*

(Received 3 June 2016; revised manuscript received 5 July 2016; published 21 September 2016)

Extensive studies have demonstrated the promising capability of the organic-inorganic hybrid halide perovskite $CH_3NH_3PbI_3$ in solar cells with a high power conversion efficiency exceeding 20%. However, the intrinsic as well as extrinsic instabilities of this material remain the major challenge to the commercialization of perovskite-based solar cells. Mixing halides is expected to resolve this problem. Here, we investigate the effect of chemical substitution in the position of the halogen atom on the structural, electronic, and optical properties of mixed halide perovskites $CH_3NH_3Pb(I_{1-x}Br_x)_3$ with a pseudocubic phase using the virtual crystal approximation method within density functional theory. With an increase of Br content x from 0.0 to 1.0, the lattice constant decreases in proportion to x with the function of $a(x) = 6.420 - 0.333x$ (Å), while the band gap and the exciton binding energy increase with the quadratic function of $E_g(x) = 1.542 + 0.374x + 0.185x^2$ (eV) and the linear function of $E_b(x) = 0.045 + 0.057x$ (eV), respectively. The photoabsorption coefficients are also calculated, showing a blueshift of the absorption onsets for higher Br contents. We calculate the phase decomposition energy of these materials and analyze the electronic charge density difference to estimate the material stability. Based on the calculated results, we suggest that the best match between efficiency and stability can be achieved at $x \approx 0.2$ in $CH_3NH_3Pb(I_{1-x}Br_x)_3$ perovskites.

DOI: 10.1103/PhysRevB.94.125139

I. INTRODUCTION

Perovskite-based solar cells (PSCs) are attracting a great deal of attention as promising devices for solar energy utilization due to a high power conversion efficiency exceeding 20% [1,2], a remarkably easy fabrication process [3–5], and low cost and a sufficient supply of raw materials [6,7]. The key component for governing the performance of PSCs is methylammonium lead tri-iodide perovskite ($CH_3NH_3PbI_3$ or $MAPbI_3$) that is used as not only a light absorber but also as a charge carrier mediator. Numerous studies reported for the past five years have confirmed that this material holds multiple desirable traits for solar cell application, such as an optimal band gap (∼1.5eV) [8], a large photoabsorption coefficient [9–11], a weak exciton binding energy (<0.05eV) [12,13], a high mobility of the free charge carrier [14–17], and an exceptionally long carrier diffusion length (>100 μm) [18]. However, it also turned out that $MAPbI_3$ may be degraded readily because of its poor material stability, which represents a significant challenge on the road to the development of commercially viable PSCs, and yet a microscopic understanding of the degradation process remains elusive [19–21].

Many experiments have demonstrated the significant impact of environmental factors on the degradation of this hybrid iodide perovskite. Niu *et al.* [19] identified the extrinsic factors causing the degradation of the perovskite film, such as moisture or oxygen, ultraviolet (UV) light, and a thermal effect. In particular, $MAPbI_3$ may be degraded easily under humid conditions, and therefore the humidity should not be over 1% in the process of device fabrication, as suggested by Grätzel and co-workers [7]. Frost *et al.* [8] proposed a series of irreversible reactions for the moisture catalyzed decomposition of $MAPbI_3$ into by-products including PbI_2(s), CH_3NH_2(aq), I_2(s), H_2(g), and H_2O. These were corroborated by measuring the x-ray diffraction (XRD) patterns before and after exposure to water [19,22,23] and with photothermal deflection spectroscopy [24]. Under illumination with UV light as well, the deterioration of PSCs occurred owing to not $MAPbI_3$ itself but to a TiO_2 scaffold, which is often used as a transporting layer for conduction electrons. Leijtens *et al.* [25] hypothesized an explanation for this phenomenon, that the electrons injected into the TiO_2 layer might be trapped in deep lying unoccupied sites. The thermal effect is also a considerable factor causing the degradation of the perovskite layer. When elevating the environmental temperature, $MAPbI_3$ may be decomposed into PbI_2 and CH_3NH_3I (or subsequently CH_3NH_2 and HI), as confirmed by several experiments [26,27]. The origin of such thermal decomposition is likely to be structural defects. It was also observed that the interface with a TiO_2 or ZnO layer plays a role in the thermal decomposition, whose mechanism was suggested to be a deprotonation of the MA cation in contact with the interface [28]. To prevent the device from moisture and UV light, multiple groups have developed encapsulation techniques, in which the device is covered by a thin glass cover slip that is sealed using a UV curable epoxy resin [29].

In addition to such extrinsic factors, Zhang *et al.* [30] reported from first-principles calculations that $MAPbI_3$ is intrinsically unstable. The authors calculated the energy change for the phase decomposition, $CH_3NH_3PbI_3 \rightarrow CH_3NH_3I + PbI_2$, showing that this reaction is exothermic and thus it may occur spontaneously even without moisture, oxygen, or UV light in the environment. Once it is formed, however, the kinetic barrier may prevent the compound from phase

*Corresponding author: ryongnam14@yahoo.com

decomposition, so that $MAPbI_3$ may still be stable for a certain period to be used safely in PSCs. Importantly, they suggested a promising method to improve the stability of PSCs: the replacement of each ingredient ion with its similar ion, i.e., I^- with Br^- or Cl^-, Pb^{2+} with Sn^{2+}, or organic $CH_3NH_3^+$ with inorganic Cs^+ [30]. In this context, it is worth noting that the efficiency as well as the operational stability of PSCs may be tuned by adjusting the structural composition and order in mixed halide perovskites [31–33].

The most favorable attempt to improve the stability of $MAPbI_3$ is to replace I ions with Br or Cl ions [32,34–36]. Noh *et al.* [32] showed that increasing the Br content x in $MAPb(I_{1-x}Br_x)_3$ causes a phase transition, e.g., from a tetragonal to a cubic phase at $x = 0.13$, and, moreover, the modification of the band gap following the quadratic function of Br content, $E_g(x) = 1.57 + 0.39x + 0.33x^2$ (eV). Most importantly, they found that for low Br concentrations ($x < 0.2$) the stability of the device was significantly improved, while the efficiency was almost unchanged. When exposed to moisture with a relative humidity of 55%, the cells underwent a significant degradation in the cases of $x = 0$ and $x = 0.06$, but for higher Br contents ($x = 0.2$ and $x = 0.29$) no large degradation was observed within the 20 day measurement period. It was suggested that this improved stability for higher Br content was attributed to a reduced lattice constant and the phase transition from a tetragonal to cubic phase. Despite such experiments, few theoretical studies based on the first-principles method to systematically investigate the improvement in stability by the substitution of Br for I could be found, to the best of our literature search.

In this paper, we aim to investigate the effects of Br substitution for I on the structural, electronic, and optical properties of mixed iodide-bromide perovskite compounds $MAPb(I_{1-x}Br_x)_3$ with a first-principles density functional theory (DFT) method. To conduct first-principles simulations of solid solutions with a moderate computational cost, we utilize the virtual crystal approximation (VCA) method [37,38] rather than the supercell method. By increasing the Br content x from 0.0 to 1.0 with an interval of 0.1, we calculate the lattice constants and band gaps, comparing with the experimental values to have confidence in the validity of the underlying VCA method. We describe a method to approximately calculate the exciton binding energy, and demonstrate a systematic variation of photoabsorption coefficients, effective masses of charge carriers, dielectric constants, and exciton binding energies in these mixed halide perovskites. Finally, we calculate the formation energies of the $MAPbX_3$ ($X = I_{1-x}Br_x$) compounds from their compositional phases MAX and PbX_2 to estimate the instabilities of these compounds, with a careful analysis of the charge density difference to assess charge transfer during the formation of the compounds.

II. METHOD

A. Exciton binding energy

To calculate the exciton binding energy, we make use of an effective mass approximation, in which an exciton made up of an electron and a hole can be viewed as a hydrogen atom. The difference between the excitonic system and the hydrogen atom is attributed to (i) a replacement of the electron and nucleus masses by the effective masses of an electron (m_e^*) in the conduction band and a hole (m_h^*) in the valence band, which can be considered to be isotropic for simplicity, and (ii) an introduction of a dielectric constant ε of the surrounding material to describe an attractive Coulomb interaction between them. Dealing with the excitonic system in the same way as solving the Schrödinger equation of a hydrogen atom gives eigenvalues of the excitonic system from which the exciton binding energy can be obtained as follows [39],

$$E_b = \frac{m_e e^4}{2(4\pi\varepsilon_0)^2\hbar^2}\frac{m_r^*}{m_e}\frac{1}{\varepsilon^2} \approx 13.56\frac{m_r^*}{m_e}\frac{1}{\varepsilon^2}(\text{eV}), \quad (1)$$

where m_r^* ($1/m_r^* = 1/m_e^* + m_h^*$) is a reduced effective mass replacing a reduced mass of the hydrogen atom μ ($1/\mu = 1/m_e + 1/m_p \approx 1/m_e$), and ε_0 is the dielectric constant of vacuum. Therefore, to calculate the exciton binding energy with this method, we need to know the dielectric constant of the material and the effective masses of the conduction electron and hole, which can be obtained through a first-principles calculation.

The validity of this exciton model, known as the *Mott-Wannier exciton* model, can be described by estimating an extending radius of the lowest bound state given as

$$a_0^* = \varepsilon\frac{m_e}{m_r^*}a_0, \quad (2)$$

where a_0 is the Bohr radius. For this model, a_0^* must be larger than the lattice constant of the crystalline solid [39]. In the case of semiconducting materials with small effective masses and large dielectric constants, it is not difficult to satisfy this requirement. Note that, when the atomic levels become more tightly bound, the exciton can become more localized, known as a *Frenkel exciton* in the extremely localized case, due to a decrease of ε and an increase of m_r^*.

B. Computational method

In this work, we carry out the DFT calculations using the pseudopotential plane-wave (PP-PW) method as implemented in the ABINIT package (version 7.10.2) [40,41]. We use a plane-wave cutoff energy of 40 Ha and a k-point mesh of $(4 \times 4 \times 4)$ for structural optimization, which guarantees a total energy convergence of 5 meV per unit cell. For the calculations of frequency-dependent dielectric constants, the electronic band structure, and the density of states (DOS), we use a denser k-point mesh of $(12 \times 12 \times 12)$.

For all the relevant atoms, we constructed the optimized norm-conserving pseudopotentials with the designed nonlocal potential as suggested by Rappe *et al.* [42] using the OPIUM package.[1] Here, the valence electronic configurations of the atoms are H $1s^1$, C $2s^22p^2$, N $2s^22p^3$, Br $4s^24p^5$, I $5s^25p^5$, and Pb $5d^{10}6s^26p^2$. To make the computational cost moderate and investigate the variation tendency when systematically

[1]The OPIUM package has features of atomic structure calculations, norm-conserving pseudopotential generation, and conversion into the fhi format, which is acceptable to the ABINIT package, and is available at http://opium.sourceforge.net.

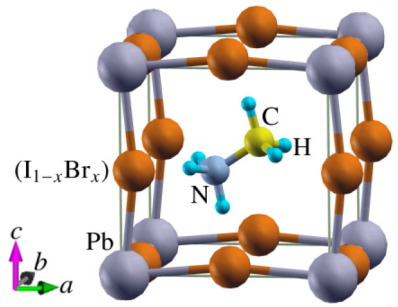

FIG. 1. Ball-and-stick model for a unit cell of mixed halide perovskites $CH_3NH_3Pb(I_{1-x}Br_x)_3$ with a pseudocubic crystalline lattice and $CH_3NH_3^+$ cation oriented to the (101) direction.

mixing the Br atom into $MAPbI_3$, we apply the virtual crystal approximation (VCA) method, using $X = I_{1-x}Br_x$ ($x = [0,1]$, the interval 0.1) as the virtual atom. To construct the pseudopotentials of these virtual atoms, we have utilized the *Yu-Emmerich extended averaging approach* (YE^2A^2 for short) proposed mainly by one of the authors (Yu) [37], which has merits to treat heterovalent atoms in a simple way and improve the accuracy of the VCA method. Throughout this work, the Perdew-Burke-Ernzerhof (PBE) [43] formalism for an exchange-correlation functional within a generalized gradient approximation (GGA) was used in the pseudopotential generation for atoms and the PP-PW calculations for crystalline solids.

The crystalline structure of $MAPb(I_{1-x}Br_x)_3$ is assumed to be pseudocubic with the Pm space group, which was identified by XRD measurements [44]. As shown in Fig. 1, the MA cation is oriented to the (101) direction, which is regarded as the lowest energetic configuration among the different orientations [11]. To determine the optimized lattice constants of the pseudocubic crystals, we calculated the total energies of the unit cells when changing the volume evenly, at which time all the atomic positions were relaxed until the atomic forces were below 0.01 eV/Å. Then, the optimized lattice constant can be obtained by fitting the E-V data into the Birch-Murnaghan equation of state [45].

Using the optimized unit cells, we calculated the frequency-dependent dielectric constants, $\varepsilon(\omega) = \varepsilon_1(\omega) + i\varepsilon_2(\omega)$, within the density functional perturbation theory (DFPT) [46]. Then, the photoabsorption coefficients as a function of frequency ω can be obtained using the following equation,[2]

$$\alpha(\omega) = \frac{2\omega}{c}\sqrt{\frac{1}{2}\left(-\varepsilon_1(\omega) + \sqrt{\varepsilon_1^2(\omega) + \varepsilon_2^2(\omega)}\right)}. \qquad (3)$$

Note that the electron-hole coupling was not considered in this work, due to a quite heavy computational cost of the scheme based on the Bethe-Salpeter equation for the two-body Green's function. However, it was known that, in the case of small band-gap materials, ignoring the electron-hole coupling still leads to quite reasonable spectra compared to experiment.

[2]See Ref. [52], in which the authors omitted the constant $2/c$ and therefore depicted the absorbance of $MAPbI_3$ in arbitrary units.

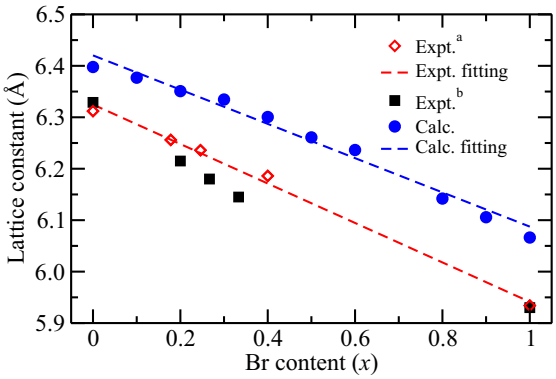

FIG. 2. Lattice constants of mixed halide perovskites $CH_3NH_3Pb(I_{1-x}Br_x)_3$ as a function of Br content x, calculated by the VCA method within DFT. Dashed lines indicate the linear fitting lines, open diamonds in red and solid squares in black represent the experimental values given in Refs. [47] and [35], and solid blue circles show the calculated values in this work, respectively.

III. RESULTS AND DISCUSSION

We first determined the optimized lattice constants of the mixed halide perovskites $MAPb(I_{1-x}Br_x)_3$ with a pseudocubic crystalline phase by estimating the E-V data and then fitting them into the Birch-Murnaghan equation of state, as described in Sec. II B. Here, the E-V data were obtained by calculating the total energy of the atomic-relaxed unit cell at each fixed volume, when increasing the volume gradually from $0.9V_0$ to $1.1V_0$, with V_0 the optimized volume. This process was repeated at each Br content x, by increasing the x from 0 to 1 with an interval of 0.1.

In Fig. 2, we show the optimized lattice constants of the $MAPb(I_{1-x}Br_x)_3$ compounds as a function of Br content x. With an increase of Br content, the lattice constants decrease almost linearly. This might be due to the partial substitution of a smaller bromine ion (ionic radius 1.96 Å) for a larger iodine ion (ionic radius 2.20 Å). It was well known that the mixed perovskites composed of two different perovskite crystals with similar lattice constants are expected to follow the Vegard's law, indicating a linear dependence of the lattice constants on the compositional order [37]. To illustrate the satisfaction of Vegard's law in the mixed halide perovskites, we interpolated the calculated lattice constants as a *linear function* of Br content x, resulting in a formula $a(x) = 6.420 - 0.333x$ (Å), which is comparable to the experimental result, $a(x) = 6.325 - 0.384x$ (Å) [47]. Although the calculated lattice constants were overestimated compared with the experimental values and thus the fitting line was overshifted in the y axis, the linear coefficient (0.333) in the fitting line to the computational data was in reasonable agreement with experiment (0.384). The deviations are on the order of 1.5%, which is typical of the PBE-GGA functional. Despite such a deviation in the magnitude of the lattice constants, the almost identical linear coefficients between calculation and experiment indicate a satisfaction of Vegard's law with the YE^2A^2.

Now we are interested in the variation tendency in electronic structures when increasing the Br content in the mixed halide perovskites $MAPb(I_{1-x}Br_x)_3$. To this end, we calculated the energy band structures and partial density of states (DOS)

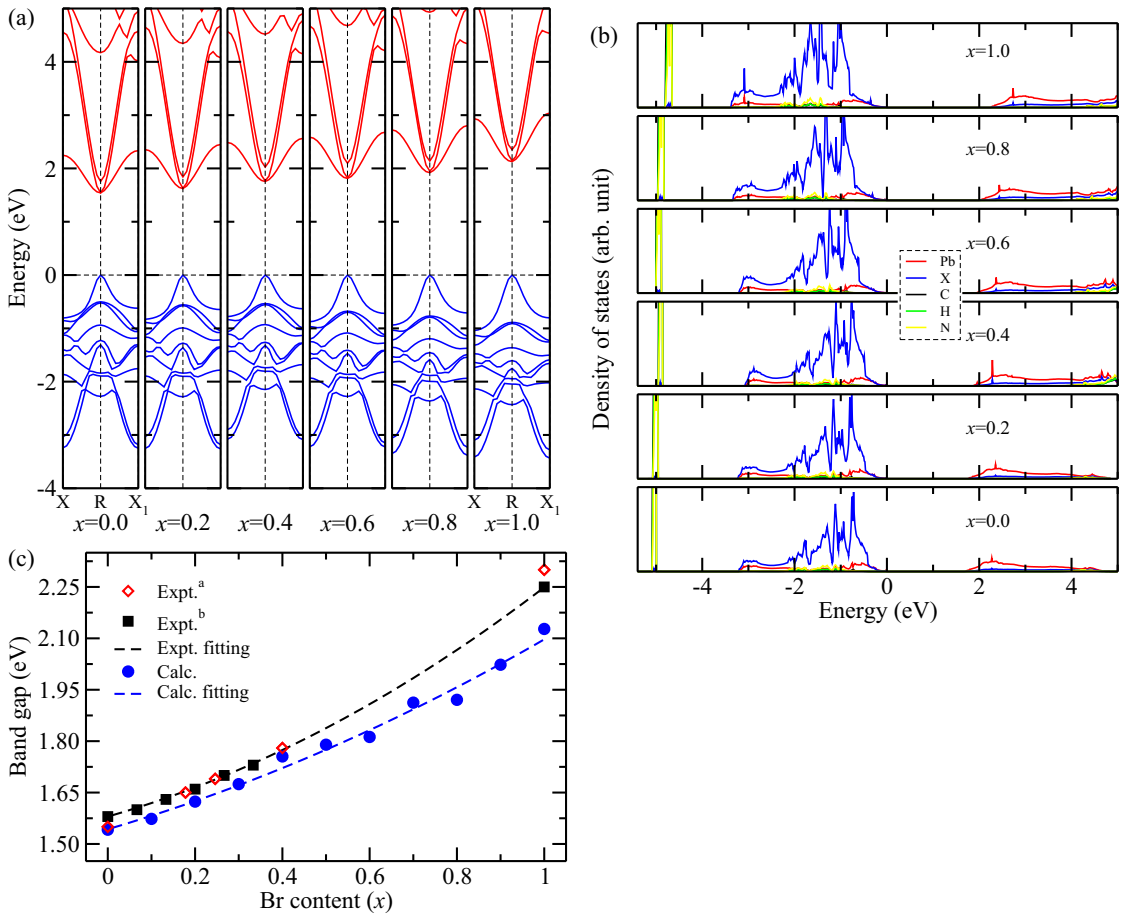

FIG. 3. Electronic structures of mixed halide perovskites $CH_3NH_3Pb(I_{1-x}Br_x)_3$ as a function of Br content x, calculated by the VCA method within DFT. (a) Electronic energy band structures around the R point, (b) atomic resolved density of states, setting the top of the valence band to zero, and (c) band gaps as a quadratic function of Br content x. X in (b) denotes virtual atoms ($I_{1-x}Br_x$). Expt.[a] and Expt.[b] data in (c) are from Refs. [47] and [35], respectively.

projected on each atom with a gradual change of Br content x, as shown in Fig. 3. We should note that the electronic band structures and DOS are gradually changed without any anomaly when increasing the Br content, again indicating a rationality of the VCA method that we have used.

We shed light on the fact that the band gaps are in a direct mode at the R point in reciprocal space over all the Br contents, as shown in Fig. 3(a). This is one of the most advantageous aspects of the mixed halide perovskites $MAPb(I_{1-x}Br_x)_3$, so that the exciton, an electron-hole pair, can be generated directly by absorption of the photons without any other process such as phonons. With respect to the magnitude of the band gaps, we can see that the calculated band gaps were slightly underestimated compared with the experimental values, with a tendency for further underestimation going from $MAPbI_3$ ($x = 0$) to $MAPbBr_3$ ($x = 1$). Nevertheless, the deviations of the band gaps from the experimental values, e.g., 0.01 eV at $x = 0$ and 0.1 eV at $x = 1$, are negligibly small, compared with other PBE-GGA calculations of inorganic semiconducting materials. This excellent agreement in the band gaps of these organic-inorganic hybrid halide perovskites could be explained by a fortuitous cancellation of errors—the GGA underestimation is counterbalanced by an overestimation due to a lack of spin-orbit coupling [48,49]. When the substitution of a lighter bromine atom ($Z = 35$) for a heavier iodine atom ($Z = 53$) occurs, the effect of spin-orbit coupling becomes weaker, and therefore a further underestimation of the band gap for $MAPbBr_3$ might not be exceptional.

Let us see the atomic resolved (and partial) DOS in detail to seek the electronic factors that are possibly responsible for the variation of the band gaps. As shown in Fig. 3(b), it was established that the valence band maximum (VBM) of $MAPbX_3$ arises predominantly from the p state of the X atom with a small contribution from the 6s state of the Pb atom, while the conduction band minimum (CBM) comes from the Pb 6p state and the X d and p states [12]. It can be thought that Br 4p states tend to hybridize more strongly with the Pb s state than with the I 5p states, causing a downshift of VBM and thus an increase of the band gap. On the other hand, although the highest occupied molecular orbitals (HOMOs) of the MA cation are found deep (∼5eV) below the VBM, having narrow features, there is a weak interaction between the organic MA cation and the inorganic PbX_6 octahedra by a possible hydrogen bonding between the ammonium group and the X atom. It is interesting to notice that, by increasing the Br content, the energy interval between the HOMO of the MA

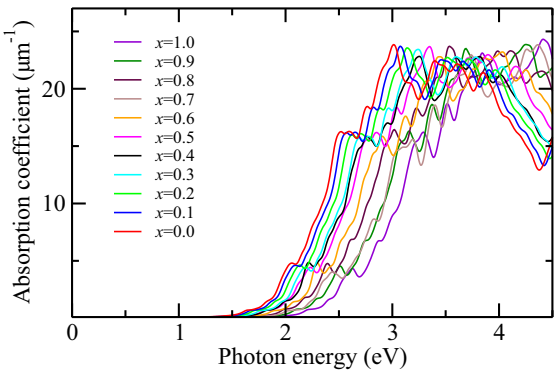

FIG. 4. Photoabsorption coefficients of mixed halide perovskites $CH_3NH_3Pb(I_{1-x}Br_x)_3$ with the increase of Br content x, calculated by the VCA and DFPT methods within DFT.

cation and the bottom level of PbX_6 is getting close, providing an indication of a stronger MA-PbX_6 interaction.

To describe the variation tendency of band gaps with increasing Br content, we also interpolated the band gaps to a *quadratic function* of Br content x as follows,

$$E_g(x) = E_g(0) + [E_g(1) - E_g(0) - b]x + bx^2, \quad (4)$$

where $E_g(0)$ and $E_g(1)$ are band gaps of $MAPbI_3$ ($x = 0$) and $MAPbBr_3$ ($x = 1$), and b is the so-called bowing parameter, respectively [35]. In Fig. 3(c), we show the result with available experimental data. Our calculation yielded the formula $E_g(x) = 1.542 + 0.374x + 0.185x^2$ (eV), i.e., $E_g(0) = 1.542$ eV, $E_g(1) = 2.101$ eV, and $b = 0.185$ eV, which are in good agreement with those from experiments, $E_g(0) = 1.58$ (1.579) eV, $E_g(1) = 2.28$ (2.248) eV, and $b = 0.33$ (0.306) eV in Ref. [32] (Ref. [35]). The bowing parameter b reflects the fluctuation degree in the crystal field and the nonlinear effect arising from the anisotropic nature of the binding [35]. Therefore, the quite small b values both in our calculation and experiments indicate a low compositional disorder and a good miscibility between $MAPbI_3$ and $MAPbBr_3$. It is clear that the substitution of a smaller bromine ion for a larger iodine ion leads to an enhancement of the interaction between Pb and X atoms in corner-sharing PbX_6 octahedra, which plays a major role in characterizing the band structure [10,50] as discussed above, and thus to a decrease of lattice constants and an increase of band gaps. The increase of band gaps implies a worsening of the light harvesting property from $MAPbI_3$ to $MAPbBr_3$, and thus a decrease of the efficiency of PSCs.

In order to directly estimate the light harvesting capability of PSCs, we next determined the photoabsorption coefficients of the mixed halide perovskites $MAPb(I_{1-x}Br_x)_3$ when increasing the Br content. These were calculated using Eq. (3) from the real and imaginary parts of the frequency-dependent dielectric constants, which were calculated within DFPT [46]. In Fig. 4, we present the photoabsorption coefficients of $MAPb(I_{1-x}Br_x)_3$ with a gradual increase of x as functions of photon energy. For lower Br contents, the perovskites exhibit an extended absorption character over the whole visible light spectrum, which is advantageous for light harvesting. For higher Br contents, however, the absorption onset gradually shifts to a higher photon energy, i.e., a shorter wavelength light,

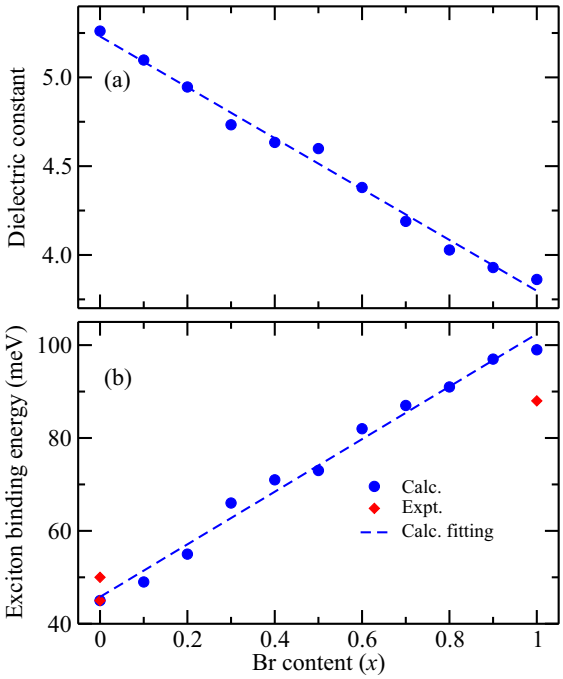

FIG. 5. (a) Dielectric constants and (b) exciton binding energies of mixed halide perovskites $CH_3NH_3Pb(I_{1-x}Br_x)_3$ when increasing the Br content x. Experimental data are from Refs. [53,54,56].

indicating a lowering of power conversion efficiency. Such a blueshift of the absorption onsets can be readily expected from the rise of band gaps in the mixed halide perovskites $MAPb(I_{1-x}Br_x)_3$ with an increase of Br content.

Another important property to be considered inevitably is the effective masses of charge carriers including the conduction electron and hole, which provide an indirect estimation of the mobility of the charge carriers. We calculated the effective masses of the conduction electron and hole by numerically processing the refined energy band data around the R point. The calculated values are $m_e^*/m_e = 0.18$ (0.21), $m_h^*/m_e = 0.19$ (0.23), and $m_r^*/m_e = 0.09$ (0.11) for $MAPbI_3$ ($MAPbBr_3$). For $MAPbI_3$ ($x = 0$), these values are comparable with the experimental values of 0.12, 0.15, and 0.09 [51], and previous theoretical values of 0.17, 0.25, and 0.11 from spin-orbit coupling GW calculations [52]. It is worth noting that the effective reduced mass (m_r^*) increases slightly from $x = 0$ to $x = 1$, indicating a worsening of charge carrier mobility when increasing the Br content.

Then we calculated the frequency-dependent dielectric constants with the DFPT method, and extracted high-frequency components. As shown in Fig. 5(a), the dielectric constants decrease monotonically when increasing the Br content x with a *linear function* of $\varepsilon(x) = 5.23 - 1.43x$. For $MAPbI_3$, the calculated value of 5.3 in this work is in reasonable agreement with recent theoretical values, 4 by the quantum molecular dynamics method [12] and 5.6–6.2 by PBEsol DFT calculation [11], and experimental values of 7–10 at 10^{12} Hz [13]. Note that the dielectric constants calculated in this work are not truly static ones, which should be higher in an order of magnitude [11], but give the most reliable exciton binding energy compared with the available experimental values, as discussed below.

Since the reduced effective masses of charge carriers and dielectric constants are in our hands, the exciton binding energy can be calculated according to Eq. (1). It plays a key role in discriminating whether charge carriers behave as free particles in normal inorganic thin-film semiconductors or as bound excitons in organic semiconductors. The weaker exciton binding energy indicates more freely behaving charge carriers. For $MAPbI_3$, the exciton binding energy was calculated to be 45 meV, with an effective exciton Bohr radius a_0^* of 3 nm, which is in good agreement with the experimental values of ~50 meV [53] and 16–45 meV [54,55]. Meanwhile, for $MAPbBr_3$, the calculated value was 99 meV with an effective exciton radius of 1.9 nm, which is also comparable with the experimental value of ~88 meV [56]. Seeing that the effective exciton Bohr radii for both cases are over their lattice constants, we can say that the excitons are likely to be of a *Mott-Wannier* type. We should note that such a good agreement in the exciton binding energy with experiment is due to taking high-frequency (optical) dielectric constants. However, as discussed in Refs. [21,57], this model is valid only if the Coulomb interaction between the conduction electron and hole, which are components of the exciton, is strong enough so that the slower lattice dielectric response does not screen the interaction. If the exciton is less strongly bound, the lower-frequency component of the dielectric constant arising from the lattice contributions (truly static ones) must be also considered. Brivio *et al.* [11] reported a static dielectric constant of up to 37 for $MAPbI_3$, which leads to a decrease of the exciton binding energy (1 meV) and an increase of the effective exciton Bohr radius (20 nm), eventually dissociating the exciton. Despite such an argument, we will rely on the values obtained by the optical dielectric constants which are close to the available experimental data, since the aim of this work is to investigate the property variation tendency when increasing the Br content.

Based on the data shown in Fig. 5(b), we know that the exciton binding energy increases in proportion to the Br content x in $MAPb(I_{1-x}Br_x)_3$, with a *linear function* of $E_b(x) = 0.045 + 0.057x$ (eV). That is, the exciton binding energies for lower Br contents, which are comparable to those of the inorganic thin-film semiconductors (<50 meV), are smaller than those for higher Br contents. This implies that, when increasing the Br content, the behavior of the charge carriers is likely to change from freelike to boundlike, causing a possible decrease of the PSC's efficiency.

To sum up the points so far, we can conclude that the substitution of the bromine atom for the iodine atom in the iodide lead perovskite $MAPbI_3$ causes a slight loss of its merits toward PSC applications. Then, what about the material stability?

To find an answer to this question, we considered the phase decomposition reaction in these mixed halide perovskites, $MAPbX_3 \rightarrow MAX + PbX_2$. The energy required for this phase decomposition reaction or the formation energy of $MAPbX_3$ from its compositions, MAX and PbX_2, could be calculated as the total energy difference as follows,

$$E_f = E_{\text{tot}}(\text{MAPb}X_3) - [E_{\text{tot}}(\text{MA}X) + E_{\text{tot}}(\text{Pb}X_2)]. \quad (5)$$

We remind that the accuracy of the formation energy should be enhanced compared with the total energy itself, since it is from the difference between the total energies of different phases, and thus an error cancellation is expected, such as 0.1 meV per formula unit in this work. The crystalline structures of MAX and PbX_2 were assumed to be the rocksalt phase with the $Fm\bar{3}m$ space group and the trigonal phase with the $P\bar{3}m1$ space group, respectively [30]. As shown in Fig. 6, the formation energies at $x = 0.0$ and $x = 0.1$ were calculated to be positive, but they became negative since $x = 0.2$ with a feature of a gradual increase of magnitude when increasing the Br content x. This result directly indicates that in the former cases the phase decompositions are exothermic, while in the latter cases they are endothermic. Therefore, it can be said that the phase decomposition of $MAPbI_3$ into MAI and PbI_2 may occur spontaneously without an application of any extrinsic factors, such as moisture or oxygen, UV light, and the thermal effect, but the phase decomposition of $MAPbBr_3$ is thermodynamically unfavorable. Our result agrees well with other PBE-GGA calculations [30]. On the experimental side, Andrei *et al.* [58] reported that the time evolution of the main XRD peak of $MAPbI_3$ showed PbI_2 peaks as soon as $MAPbI_3$ was formed, while for $MAPbBr_3$ there was no evidence of a $PbBr_2$ peak. From our calculation results, which agreed well with other calculations and experiments, we can conclude that the material stability of $MAPb(I_{1-x}Br_x)_3$ can be enhanced systematically by increasing the Br content, and, most interestingly, the mixed halide perovskites $MAPb(I_{1-x}Br_x)_3$ become intrinsically stable since $x \approx 0.2$.

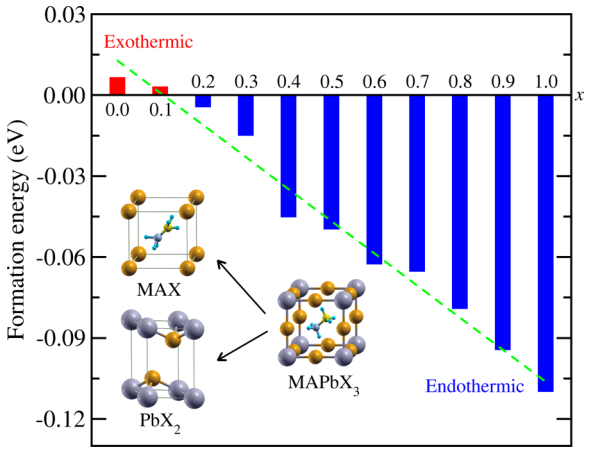

FIG. 6. Formation energies of mixed halide perovskites $CH_3NH_3PbX_3$ ($X = I_{1-x}Br_x$) from their components CH_3NH_3X and PbX_2 when increasing the Br content x. The green dotted line indicates a linear fitting.

In order to obtain intuitive insights into charge transfer in the event of compound formation and chemical bonding characteristics, we calculated the electronic charge density difference between the $MAPbX_3$ and PbX_3 framework plus MA molecule as follows,

$$\Delta n(\boldsymbol{r}) = n_{\text{MAPb}X_3}(\boldsymbol{r}) - [n_{\text{Pb}X_3}(\boldsymbol{r}) + n_{\text{MA}}(\boldsymbol{r})]. \quad (6)$$

In Fig. 7, we show the calculated electronic charge density differences only at $x = 0.0, 0.5$, and 1.0 for a clear comparison. In the middle panel of Fig. 7, we can see that much charge accumulation has occurred in the interspatial region surrounding the halogen atom, while charge depletions have

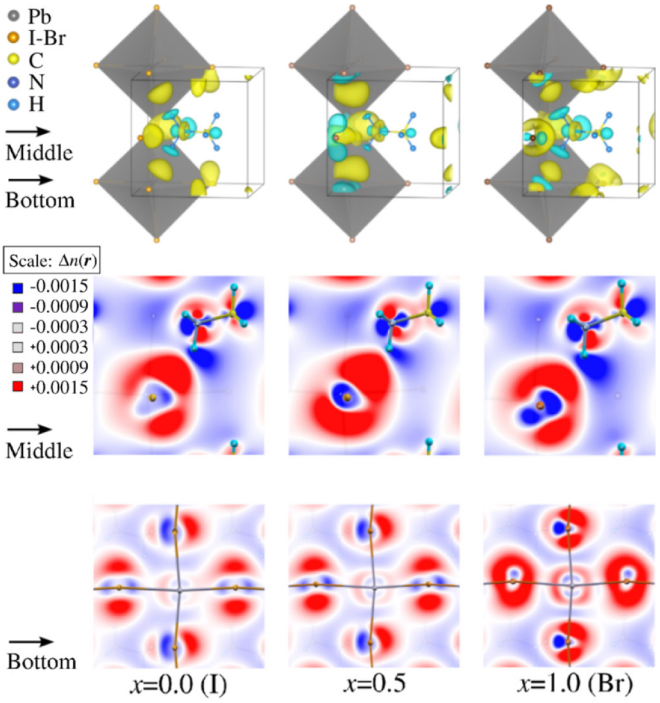

FIG. 7. Electronic charge density differences of mixed halide perovskites $CH_3NH_3Pb(I_{1-x}Br_x)_3$ at the Br contents $x = 0.0$, 0.5, and 1.0. The upper panel shows three-dimensional (3D) isosurface plots evaluated at a value of ± 0.0015 $|e|/\text{Å}^3$, where the yellow (blue) color represents positive (negative) values, indicating electron accumulation (depletion), and the middle and lower panels show two-dimensional (2D) isoline plots on the middle plane containing a $CH_3NH_3^+$ cation and a halogen atom (indicated by the blue arrow) and on the bottom plane containing Pb and halogen atoms (indicated by the red arrow), respectively.

occurred in the region around the hydrogen atom of the MA cation and in the vicinity close to the halogen atom. In the lower panel, meanwhile, great and weak charge accumulations are shown around the halogen atom and the Pb atom, and charge depletion has occurred in the localized region close to the halogen atom. These indicate that the electrons are in general transferred from the MA molecule and the Pb atom to the halogen atom, making the chemical bond strong. We can also see that, overall, the charge transferring is gradually enhanced going from I to Br, indicating that the chemical bond becomes stronger from I to Br. This agrees well with our previous observation that the lattice constants decrease with an increase of Br content.

These computational results are correlated with the experimental findings that at the experimental condition the compounds at $x = 0.2$ or $x = 0.29$ remained quite stable for tens of days, while at $x = 0.0$ and $x = 0.06$ they were degraded severely within a few days [20,32]. Together with the fact that the efficiency is not much spoiled at $x \approx 0.2$ with a band gap of 1.62 eV and an exciton binding energy of 55 meV in this work, and as confirmed by experiment [32], we can suggest that the best match between efficiency and stability can be realized at $x \approx 0.2$ in the mixed halide perovskites $MAPb(I_{1-x}Br_x)_3$.

IV. CONCLUSION

Despite the remarkable advances in the performance of hybrid halide perovskites, the degradation and instability in these materials still remain as barriers to their practical use in solar cell applications. In this work, using the VCA method within DFT, we have investigated the influence of halide composition on the structural, electronic, and optical properties of the mixed halide perovskites $MAPb(I_{1-x}Br_x)_3$. When increasing the Br content x from 0.0 to 1.0, we have found a decrease of lattice constants with a linear function of $a(x) = 6.420 - 0.333x$ (Å), while we found a increase of band gaps and exciton binding energies with a quadratic function of $E_g(x) = 1.542 + 0.374x + 0.185x^2$ (eV) and a linear function of $E_b(x) = 0.045 + 0.057x$ (eV), respectively. The increase of band gaps with increasing Br content is due to the stronger hybridization of the Br $4p$ states with the Pb s states than with the I $5p$ states, which leads to a downshift of VBM, accompanied by a decrease of the lattice constant. When increasing the Br content, the energy interval between the HOMO of the MA cation and the bottom level of PbX_6 is getting close, providing an indication of becoming a stronger MA-PbX_6 interaction. The calculated photoabsorption coefficients exhibit a blueshift of the absorption onsets for higher Br content. The substitution of the Br atom for the I atom leads to an enhancement of the stability, which was described by analyzing the energy change of the phase decomposition reaction and electronic charge density difference. In conclusion, our work leads to the suggestion that, considering the tunability of material properties by adjusting the Br content x in the mixed halide perovskites $MAPb(I_{1-x}Br_x)_3$, the best match between efficiency and stability might be achieved at $x \approx 0.2$, which is a turning point from the unstable to stable phase with maximally possible efficiency.

ACKNOWLEDGMENTS

This work was supported partially from the Committee of Education, Democratic People's Republic of Korea, under the project entitled "Strong correlation phenomena at superhard, superconducting and nano materials" (Grant No. 02-2014). The simulations have been carried out on the HP Blade System c7000 (HP BL460c) that is owned and managed by the Faculty of Materials Science, Kim Il Sung University.

[1] H. Zhou, Q. Chen, G. Li, S. Luo, T.-B. Song, H.-S. Duan, Z. Hong, J. You, Y. Liu, and Y. Yang, Science **345**, 542 (2014).
[2] N. J. Jeon, J. H. Noh, W. S. Yang, Y. C. Kim, S. Ryu, J. Seo, and S. I. Seok, Nature (London) **517**, 476 (2015).
[3] J. Liu, J. Lin, Q. Xue, Q. Ye, X. He, L. Ouyang, D. Zhuang, C. Liao, H. L. Yip, J. Mei *et al.*, J. Power Sources **301**, 242 (2016).
[4] M. Liu, M. B. Johnston, and H. J. Snaith, Nature (London) **501**, 395 (2013).

[5] S. Casaluci, L. Cinà, A. Pockett, P. S. Kubiak, R. G. Niemann, A. Reale, A. D. Carlo, and P. J. Cameron, J. Power Sources **297**, 504 (2015).

[6] F. D. Giacomo, S. Razza, F. Matteocci, A. D'Epifanio, S. Licoccia, T. M. Brown, and A. D. Carlo, J. Power Sources **251**, 152 (2014).

[7] J. Burschka, N. Pellet, S. J. Moon, R. Humphry-Baker, P. Gao, M. K. Nazeeruddin, and M. Grätzel, Nature (London) **499**, 316 (2013).

[8] J. M. Frost, K. T. Butler, F. Brivio, C. H. Hendon, M. van Schilfgaarde, and A. Walsh, Nano Lett. **14**, 2584 (2014).

[9] R. Lindblad, D. Bi, B.-w. Park, J. Oscarsson, M. Gorgoi, H. Siegbahn, M. Odelius, E. M. J. Johansson, and H. Rensmo, J. Phys. Chem. Lett. **5**, 648 (2014).

[10] J. Even, L. Pedesseau, J.-M. Jancu, and C. Katan, J. Phys. Chem. Lett. **4**, 2999 (2013).

[11] F. Brivio, A. B. Walker, and A. Walsh, APL Mater. **1**, 042111 (2013).

[12] T. Hakamata, K. Shimamura, F. Shimojo, R. K. Kalia, A. Nakano, and P. Vashishta, Sci. Rep. **6**, 19599 (2016).

[13] S. D. Stranks and H. J. Snaith, Nat. Nanotechnol. **10**, 391 (2015).

[14] E. Edri, S. Kirmayer, S. Mukhopadhyay, K. Gartsman, G. Hodes, and D. Cahen, Nat. Commun. **5**, 3461 (2014).

[15] Q. Lin, A. Armin, R. C. R. Nagiri, P. L. Burn, and P. Meredith, Nat. Photonics **9**, 106 (2014).

[16] J. S. Manser and P. V. Kamat, Nat. Photonics **8**, 737 (2014).

[17] Y. Yamada, T. Nakamura, M. Endo, A. Wakamiya, and Y. Kanemitsu, J. Am. Chem. Soc. **136**, 11610 (2014).

[18] S. D. Stranks, G. E. Eperon, G. Grancini, C. Menelaou, M. J. P. Alcocer, T. Leijtens, L. M. Herz, A. Petrozza, and H. J. Snaith, Science **342**, 341 (2013).

[19] G. Niu, X. Guo, and L. Wang, J. Mater. Chem. A **3**, 8970 (2015).

[20] D. Wang, M. Wright, N. K. Elumalai, and A. Uddin, Sol. Energy Mater. Sol. Cells **147**, 255 (2016).

[21] Z. Xiao, Y. Yuan, Q. Wang, Y. Shao, Y. Bai, Y. Deng, Q. Dong, M. Hu, C. Bi, and J. Huang, Mater. Sci. Eng., R **101**, 1 (2016).

[22] J. Yang, B. D. Siempelkamp, D. Liu, and T. L. Kelly, ACS Nano **9**, 1955 (2015).

[23] J. A. Christians, P. A. M. Herrera, and P. Kamat, J. Am. Chem. Soc. **137**, 1530 (2015).

[24] S. D. Wolf, J. Holovsky, S. J. Moon, P. Loper, B. Niesen, M. Ledinsky, F. J. Haug, J. H. Yum, and C. Ballif, J. Phys. Chem. Lett. **5**, 1035 (2014).

[25] T. Leijtens, G. E. Eperon, S. Pathak, A. Abate, M. M. Lee, and H. J. Snaith, Nat. Commun. **4**, 2885 (2013).

[26] A. Dualeh, P. Gao, S. I. Seok, M. K. Nazeeruddin, and M. Grätzel, Chem. Mater. **26**, 6160 (2014).

[27] B. Conings, J. Drijkoningen, N. Gauquelin, A. Babayigit, J. D'Haen, L. D'Olieslaeger, A. Ethirajan, J. Verbeeck, J. Manca, E. Mosconi *et al.*, Adv. Energy Mater. **5**, 1500477 (2015).

[28] J. Yang, B. D. Siempelkamp, E. Mosconi, F. D. Angelis, and T. L. Kelly, Chem. Mater. **27**, 4229 (2015).

[29] Y. Han, S. Meyer, Y. Dkhissi, K. Weber, J. Pringle, U. Bach, L. Spiccia, and Y.-B. Cheng, J. Mater. Chem. A **3**, 8139 (2015).

[30] Y.-Y. Zhang, S. Chen, P. Xu, H. Xiang, X.-G. Gong, A. Walsh, and S.-H. Wei, arXiv:1506.01301.

[31] E. Mosconi, A. Amat, M. K. Nazeeruddin, M. Grätzel, and F. D. Angelis, J. Phys. Chem. C **117**, 13902 (2013).

[32] J. H. Noh, S. H. Im, J. H. Heo, T. N. Mandal, and S. I. Seok, Nano Lett. **13**, 1764 (2013).

[33] S. Aharon, B. E. Cohen, and L. Etgar, J. Phys. Chem. C **118**, 17160 (2014).

[34] A. Sadhanala, F. Deschler, T. H. Thomas, S. E. Dutton, K. C. Goedel, F. C. Hanusch, M. L. Lai, U. Steiner, T. Bein, P. Docampo *et al.*, J. Phys. Chem. Lett. **5**, 2501 (2014).

[35] L. Atourki, E. Vega, B. Marì, M. Mollarb, H. A. Ahsainec, K. Bouabida, and A. Ihlal, Appl. Surf. Sci. **371**, 112 (2016).

[36] W. Zhu, C. Bao, F. Li, T. Yu, H. Gao, Y. Yi, J. Yang, G. Fu, X. Zhou, and Z. Zou, Nano Energy **19**, 17 (2016).

[37] C.-J. Yu and H. Emmerich, J. Phys.: Condens. Matter **19**, 306203 (2007).

[38] J. Iniguez, D. Vanderbilt, and L. Bellaiche, Phys. Rev. B **67**, 224107 (2003).

[39] N. W. Ashcroft and N. D. Mermin, *Solid State Physics* (Saunders College Publishing and Harcourt College Publishers, Orlando, FL, 1979).

[40] X. Gonze, B. Amadon, P. M. Angladeet *al.*, Comput. Phys. Commun. **180**, 2582 (2009).

[41] X. Gonze, G.-M. Rignanese, M. Verstraeteet *al.*, Z. Kristallogr. **220**, 558 (2005).

[42] A. M. Rappe, K. M. Rabe, E. Kaxiras, and J. D. Joannopoulos, Phys. Rev. B **41**, 1227 (1990).

[43] J. P. Perdew, K. Burke, and M. Ernzerhof, Phys. Rev. Lett. **77**, 3865 (1996).

[44] T. Baikie, Y. Fang, J. M. Kadro, M. Schreyer, F. Wei, S. G. Mhaisalkar, M. Grätzel, and T. J. White, J. Mater. Chem. A **1**, 5628 (2013).

[45] F. Birch, Phys. Rev. **71**, 809 (1947).

[46] S. Sharma, J. K. Dewhurst, and C. Ambrosch-Draxl, Phys. Rev. B **67**, 165332 (2003).

[47] R. K. Misra, L. Ciammaruchi, S. Aharon, D. Mogilyansky, L. Etgar, I. Visoly-Fisher, and E. A. Katz, arXiv:1603.08683.

[48] C. Motta, F. El-Mellouhi, S. Kais, N. Tabet, F. Alharbi, and S. Sanvito, Nat. Commun. **6**, 7026 (2015).

[49] C.-J. Yu, U.-G. Jong, M.-H. Ri, G.-C. Ri, and Y.-H. Pae, J. Mater. Sci. **51**, 9849 (2016).

[50] M. A. Green, A. Ho-Baillie, and H. J. Snaith, Nat. Photonics **8**, 506 (2014).

[51] K. Tanaka, T. Takahashi, T. Ban, T. Kondo, K. Uchida, and N. Miura, Solid State Commun. **127**, 619 (2003).

[52] P. Umari, E. Mosconi, and F. D. Angelis, Sci. Rep. **4**, 4467 (2014).

[53] V. D'Innocenzo, G. Grancini, M. J. P. Alcocer, A. R. S. Kandada, S. D. Stranks, M. M. Lee, G. Lanzani, H. J. Snaith, and A. Petrozza, Nat. Commun. **5**, 3486 (2014).

[54] T. C. Sum and N. Mathews, Energy Environ. Sci. **7**, 2518 (2014).

[55] A. Miyata, A. Mitioglu, P. Plochocka, O. Portugall, and R. J. Nicholas, Nat. Phys. **11**, 582 (2015).

[56] D. Moses, J. Wang, A. Heeger, N. Kirova, and S. Brazovski, Proc. Natl. Acad. Sci. USA **98**, 13496 (2001).

[57] G. Grancini, A. R. S. Kandada, J. M. Frostet *al.*, Nat. Photonics **9**, 695 (2015).

[58] A. Buin, R. Comin, J. Xu, A. H. Ip, and E. H. Sargent, Chem. Mater. **27**, 4405 (2015).